ANZIAM J. 57(2015), 43–61
doi:10.1017/S1446181115000152

ANALYTICAL REPRESENTATIONS OF REGULAR-SHAPED NANOSTRUCTURES FOR GAS STORAGE APPLICATIONS

WEI-XIAN LIM[1] and AARON W. THORNTON✉[2]

(Received 23 April, 2012; accepted 13 May, 2015; first published online 2 September 2015)

Abstract

Nanospace governs the dynamics of physical, chemical, material and biological systems, and the facility to model it with analytical formulae provides an essential tool to address some of the worlds' key problems such as gas purification, separation and storage. This paper aims to provide some analytical models to exploit building blocks representing various geometric shapes that describe nanostructures. In order to formulate the various building blocks, we use the continuous approximation which assumes a uniform distribution of atoms on their surfaces. We then calculate the potential energy of the van der Waals interaction between an atom and the structure to evaluate the location of the atom where the potential energy is at its minimum. We provide applications of the analytical models for some real structures where more than one type of building block is required.

2010 *Mathematics subject classification*: 5100.

Keywords and phrases: gas storage, potential energy, van der Waals potential, nanostructures, building blocks.

1. Introduction

Nanospace is the term used to describe the realm of nanoscaled objects. The interactions of these objects govern the dynamics of many physical, chemical, material and biological systems. Here we review some of the work related to the continuous approximation which assumes that discrete atomic structures can be smeared over lines or surfaces using average atomic densities. This approximation leads to analytical formulae for interaction energies. Through the modelling of nanospace with analytical formulae, we may address problems in the field of nanotechnology including (but not limited to) gas purification and separation for clean energy purposes, and energy-efficient, environmentally safe methods for storing gas. We aim to understand the

[1]Nanomechanics Group, School of Mathematical Sciences, University of Adelaide, South Australia 5005, Australia.
[2]CSIRO Materials Science and Engineering, Private Bag 33, Clayton South MDC, Victoria 3169, Australia; e-mail: aaron.thornton@csiro.au.

nature of interaction energies in order to grasp the most efficient configuration in nanospace. Our ability to build high-performing adsorbents can be greatly improved by using a mathematical model that explains the interaction of gases with adsorbents at the nanoscale.

Porous nanostructures such as carbon-based structures [3] and metal-organic frameworks (MOFs) [11] which are highly ordered and periodic, have been shown to be the most efficient for gas storage, since they possess low densities, large surface areas and tunable pore sizes [9], and they rely on physisorption which means that adsorbents are adsorbed on the surface of these structures through weak interactions. Current methods of gas storage such as high-pressure tanks and metal hydrides are unfavourable as the former can be energy- and space-inefficient [2], and the latter relies on the chemisorption process (where the adsorbent is chemically bonded within host hydrides) which suffers from high operating temperature, slow kinetics and low gravimetric storage [12]. Porous materials which rely on physisorption are also effective for gas separation processes due to the molecular sieving effect, where the pore size of the structure determines whether the gas can enter the pores. The packing interactions between the adsorbate and the surface of the adsorbent contribute to the ability of the material to selectively adsorb gases [6].

There has been a lot of research to develop an improved understanding of the adsorption process and optimize the conditions for gas storage and separation; for example, see the paper by Watanabe and Sholl [16]. In that paper, the adsorption and diffusion behaviour of CO_2/N_2 gas mixtures in 1163 MOFs are predicted using the classical molecular simulation. Some selected materials are then analysed to provide information about the flexibility of the structure and their chemical interactions with contaminants. Although computational simulations are currently the preferred methods to explore the properties of porous materials due to their capacity to be highly accurate, analytical models are less time-consuming, and do not require considerable computing power. In addition, applied mathematical modelling has been shown to produce results that are comparable with computer simulations and existing experimental data [7, 13].

Thornton et al. [13] analytically evaluated the heat of adsorption for MOF-177 and its gravimetric and volumetric uptake capacities for hydrogen and methane gas adsorption. The modelling output for total hydrogen uptake provided good agreement with various experimental and simulation results in the literature which ensures the accuracy of the predictions made. A similar analytical method is also employed by Lim et al. [7] to explore the hydrogen adsorption on beryllium benzene tribenzoate (Be-BTB). The hydrogen adsorption isotherm calculated using their proposed analytical model closely matches the data obtained from experiments and simulations at 77 and 298 K. Using that model, the authors reached the same conclusions as the results obtained in the literature, that is, there is a correlation between hydrogen uptake and both surface area and pore volume at high pressure.

In this paper, we represent both simple and complicated geometries of nanoporous materials using idealized building blocks that describe the interactions with simple

https://doi.org/10.1017/S1446181115000152 Published online by Cambridge University Press

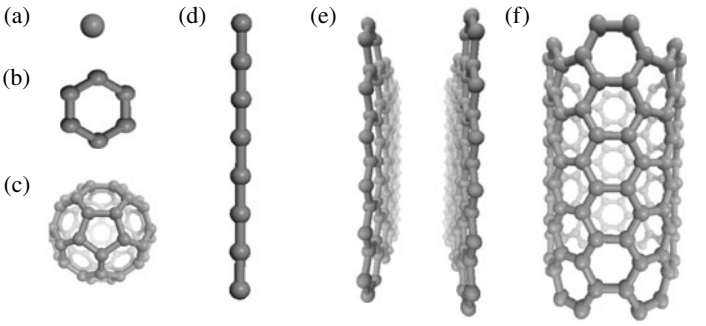

FIGURE 1. Various atomic representations of structures that can be idealized by building blocks. An atom can be described by a point (a), benzene by a ring (b), fullerene as a sphere (c), a carbon chain by a line (d), graphene sheets by planes (e), and a carbon nanotube by a cylinder (f).

and elegant analytical models. Section 2 introduces the analytic representations of the van der Waals interaction between an atom and building blocks which are represented by standard geometrical shapes such as points, lines, planes, spheres and cylinders as shown in Figure 1. Section 3 then discusses some examples of how they can be exploited to describe actual nanostructures and a brief conclusion is given in Section 4.

2. Interaction points with building blocks

In this section, we first introduce some methods which can be used to describe the van der Waals energy that exists between an atom interacting with a nanostructure. There are several methods that can be used to calculate the total interaction energy of atom P interacting with nanostructure J. If the locations of P and the atoms on J (which are denoted as j) are known, and are defined by coordinate positions, we can evaluate the total interaction energy U by calculating the sum of the individual atomic interactions between j and P; thus

$$U = \sum_j \Phi(\rho_{jp}),$$

where $\Phi(\rho)$ is the potential energy function, and ρ_{jP} is the distance between atoms j and P.

If J is large or the locations of its atoms are not known, the discrete method can be replaced by the continuum approximation provided that the geometry is reasonably simple, such as cylinders for nanotubes and spherical surfaces for fullerenes. Using this method, we assume that the atoms on the surface are uniformly distributed so that we can perform a continuous integration over the surface to obtain the total interaction energy

$$U = \eta_J \int_{S_J} \Phi(\rho)\, dS_J, \tag{2.1}$$

https://doi.org/10.1017/S1446181115000152 Published online by Cambridge University Press

where η_J denotes the atomic density (number of atoms/surface area) on surface J and ρ represents the distance between P and the surface element dS_J.

The interaction energy between two atoms can be described by various potential functions. In this paper, we focus on the 6–12 Lennard-Jones potential [5] which describes the interaction between two nonbonded atoms. Using the Lennard-Jones potential, we describe the interaction between j and P as

$$\Phi(\rho) = -\frac{C_1}{\rho^6} + \frac{C_2}{\rho^{12}},$$

where $C_1 = 4\epsilon\sigma^6$ and $C_2 = 4\epsilon\sigma^{12}$ represent the attractive constant and the repulsive constant, respectively, with ϵ as the well depth and σ as the van der Waals diameter obtained by Rappe et al. [10].

Nanostructures can be quite complicated and difficult to represent geometrically, but they can be represented in a simple manner by introducing the idea of *building blocks*. Due to the symmetric nature of the building blocks that we introduce, the interaction energy between an arbitrary point and these building blocks can be modelled using the continuum approximation and a simplified version of equation (2.1). Thus,

$$U = \eta_J(-C_1 R_3 + C_2 R_6), \tag{2.2}$$

where

$$R_n = \int_{S_J} \frac{1}{\rho^{2n}}\, dS_J \tag{2.3}$$

with $n = 3$ and 6. In the following subsections, we present the interaction energy between an arbitrary point and various building blocks using this approach.

2.1. Interaction with a point Given the coordinates of two atoms, atom $P = (x_p, y_p, z_p)$ and atom $j = (x_j, y_j, z_j)$, the parameter ρ in equation (2.3) is given by

$$\rho = [(x_p - x_j)^2 + (y_p - y_j)^2 + (z_p + z_j)^2]^{1/2},$$

which is the formula for the distance between the location of j and P.

2.1.1. Carbon In this section, we use equation (2.2) to calculate the potential energy between a carbon (C) atom and a hydrogen (H) atom. We assumed that C is located at the origin $(0, 0, 0)$ and H is located at $(0, y_1, z_1)$. Figures 2(a) and (b) show the contour plots for C interacting with H in two and three dimensions, respectively. The figures show that the hydrogen atom is most stable at a distance of 3.3 Å from the carbon atom, as shown by the blue area (colour online) of the contour plots which defines the minimum potential energy. The parameter values used to obtain our figures are as given in Table 1.

https://doi.org/10.1017/S1446181115000152 Published online by Cambridge University Press

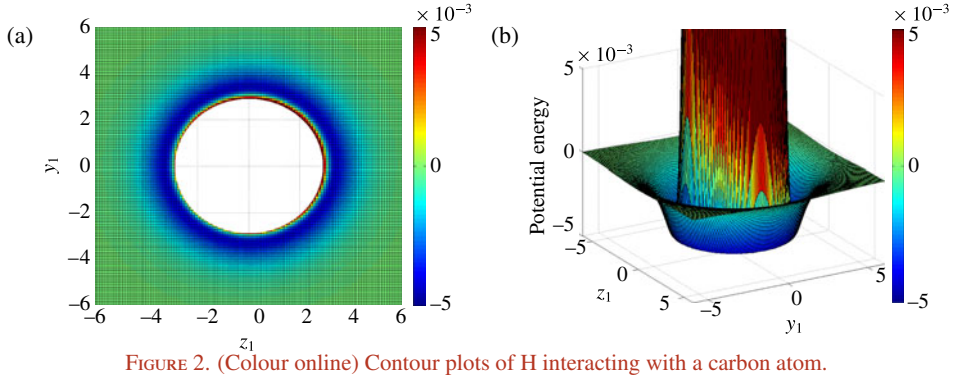

FIGURE 2. (Colour online) Contour plots of H interacting with a carbon atom.

TABLE 1. Numerical values of various parameters (H–C denotes the interaction between hydrogen and carbon, and H–H denotes the interaction between hydrogen and hydrogen).

Parameter	Description	Value
r_c	radius of C ring (benzene)	1.4 Å
r_h	radius of H ring (benzene)	2.48 Å
t	radius of fullerene	3.55 Å
c	radius of (10,10) carbon nanotube	6.784 Å
η_2	mean atomic density of C and H in polyacetylene	0.831 Å^{-2}
η_3	mean atomic density of graphene	0.382 Å^{-2}
η_{4c}	mean atomic density of C ring (benzene)	0.682 Å^{-2}
η_{4h}	mean atomic density of H ring (benzene)	0.385 Å^{-2}
η_5	mean atomic density of fullerene	0.379 Å^{-2}
η_6	mean atomic density of carbon nanotube	0.381 Å^{-2}
$C_{1\ \mathrm{H–C}}$	attractive constant H–C	5.576 eVÅ^6
$C_{1\ \mathrm{H–H}}$	attractive constant H–H	1.036 eVÅ^6
$C_{2\ \mathrm{H–C}}$	repulsive constant H–C	3944.302 eVÅ^{12}
$C_{2\ \mathrm{H–H}}$	repulsive constant H–H	208.178 eVÅ^{12}

2.2. Interaction with a line Using a two-dimensional coordinate system, the line L lies on the x-axis and any position on L is denoted by $(0, t)$. Point P is located at $(g, 0)$ and the distance between P and L is given by

$$\rho = [g^2 + t^2]^{1/2}.$$

Given the line element dt, we solve equation (2.3) to obtain

$$R_n = \int_{-\infty}^{\infty} (g^2 + t^2)^{-n}\, dt$$
$$= g^{1-2n} B\left(\frac{1}{2}, n - \frac{1}{2}\right).$$

https://doi.org/10.1017/S1446181115000152 Published online by Cambridge University Press

R_n is then substituted into equation (2.2) to yield the potential energy for L and P,

$$U_{LP} = \eta\pi\left(-\frac{3C_1}{8g^5} + \frac{63C_2}{256g^{11}}\right), \tag{2.4}$$

where η is the mean atomic density of line L calculated by dividing the number of atoms by the length of the line, and $B(x, y)$ is the beta function such that

$$B(x, y) = \frac{(x-1)!(y-1)!}{(x+y-1)!}.$$

If the coordinates are known such that $P = (x_p, y_p, z_p)$ and two points located on the line L are $L_1 = (x_1, y_1, z_1)$ and $L_2 = (x_2, y_2, z_2)$, the parameter g in equation (2.4) can be replaced by

$$g = \frac{|(L_1 - P) \times (L_2 - L_1)|}{|(L_2 - L_1)|},$$

which is the shortest distance between P and L.

2.2.1. Polyacetylene This section describes the interaction of a hydrogen atom with polyacetylene which is an organic polymer with the repeating unit $(C_2H_2)_n$ that creates a long polymer chain. We assume that the hydrogen atom lies at the location $(0, y_2, z_2)$. The polyacetylene is located on the x-axis and the two locations on the line (picked at random) are $L_1 = (3, 0, 0)$ and $L_2 = (-2, 0, 0)$ which represent two atoms in the chain. The total potential energy between the hydrogen atom and polyacetylene is calculated by adding up the potential energies for H interacting with the hydrogen line and carbon line to yield

$$U_{\text{tot}} = U_C + U_H, \tag{2.5}$$

where U_C is the potential energy for H with the carbon line and U_H is the potential energy for H with the hydrogen line. The value of parameters C_1 and C_2 for both the hydrogen–carbon and hydrogen–hydrogen interactions can be found in Table 1. To calculate the mean line density, we found the length of a particular section of the polyacetylene, $C_{10}H_{10}$ (as shown in Figure 3) to be 12.027 Å. The mean line density for carbon and hydrogen for the polyacetylene (η_2) is then obtained by dividing the corresponding number of atoms by its length to obtain $10/12.027 = 0.831$ Å^{-2}. The blue area in Figures 4(a) and (b) (colour online) represents the minimum potential energy. This shows that the hydrogen atom is most stable at a distance of about 3.2 Å from the polyacetylene.

2.3. Interaction with a plane We now consider the interaction of a plane S with a point P using a three-dimensional coordinate system. We assume that S lies on the yz-plane, S_P lies on the plane S and P lies on the x-axis. Given that $S_P = (0, u, v)$ and $P = (g, 0, 0)$, where g is the perpendicular distance of P from S, the distance between P and S is given by

$$\rho = [g^2 + u^2 + v^2]^{1/2}.$$

https://doi.org/10.1017/S1446181115000152 Published online by Cambridge University Press

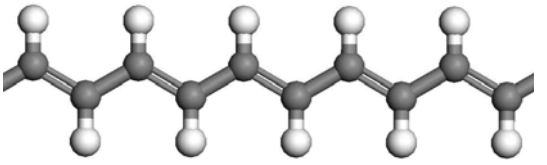

FIGURE 3. Structure of polyacetylene ($C_{10}H_{10}$).

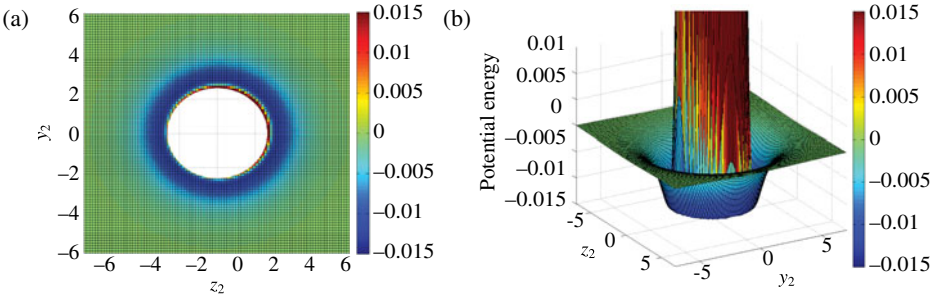

FIGURE 4. (Colour online) Contour plots of H interacting with the carbon atoms on polyacetylene.

Using $du\,dv$ as the area element of the plane, R_n is given by

$$R_n = \int_{-\infty}^{\infty}\int_{-\infty}^{\infty}(g^2+u^2+v^2)^{-n}\,du\,dv$$
$$= g^{2-2n}B\left(n-\frac{1}{2},\frac{1}{2}\right)B\left(n-1,\frac{1}{2}\right).$$

The total interaction energy between P and S_P is given by

$$U_{PS} = \pi\eta\left(-\frac{C_1}{2g^4}+\frac{C_2}{5g^{10}}\right), \tag{2.6}$$

where η is the mean atomic density.

Similarly to Section 2.2, we can replace the parameter g with the shortest distance from P to S if the coordinates are given such that $P=(x_p,y_p,z_p)$, and three points located on S are $S_1=(x_1,y_1,z_1)$, $S_2=(x_2,y_2,z_2)$ and $S_3=(x_3,y_3,z_3)$. The shortest distance is thus defined as

$$g = \hat{n}\cdot(P-S_x), \tag{2.7}$$

where S_x is any of the points S_1, S_2, S_3 and

$$\hat{n} = \frac{(S_2-S_1)\times(S_3-S_1)}{|(S_2-S_1)\times(S_3-S_1)|}$$

is the unit normal for S.

https://doi.org/10.1017/S1446181115000152 Published online by Cambridge University Press

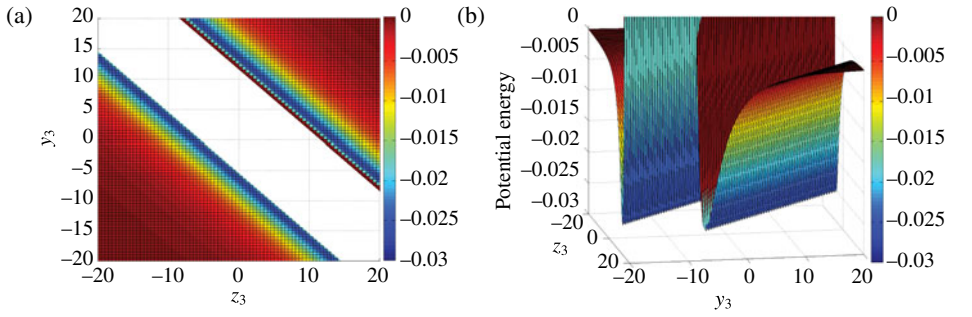

FIGURE 5. (Colour online) Contour plots of H interacting with a graphene sheet.

2.3.1. Graphene sheet We present the case of a hydrogen atom interacting with a sheet of graphite in this section. The mean surface density for a graphene sheet is denoted by $\eta_3 = 4\sqrt{3}/(9\gamma^2)$, where γ is the carbon–carbon bond length. For a sheet of graphene, $\gamma = 1.42$ Å so that $\eta_3 = 0.382\,\text{Å}^{-2}$. The parameters C_1 and C_2 for the hydrogen–carbon interactions can be found in Table 1. We assume that the locations of three points on the plane (picked at random) are $S_1 = (1, 2, 4)$, $S_2 = (2, 4, 5)$ and $S_3 = (3, 5, 7)$ and the location of the hydrogen atom is $P = (0, y_3, z_3)$.

Substituting P, S_1, S_2 and S_3 into equation (2.7) will provide the shortest distance, and g is then substituted in equation (2.6). The potential energy between S and P against varying values of y_3 and z_3 is plotted in Figures 5(a) and (b). We can observe that the minimum potential energy is located at the dark blue section (colour online) of the contour plots. The hydrogen atom is stable when it is about 3 Å distance away from the graphene sheet.

2.4. Interaction with a ring

In this section, we will introduce the analytic formulae for the interaction between a point and a ring. This interaction can be categorized into two cases: (i) the point is interacting with the ring from the side; and (ii) the point is interacting with the ring from the top or bottom. These two cases will be discussed in this section.

2.4.1. Point P located at the side of the ring In this case, we use a two-dimensional coordinate system with the centre of ring Q of radius q located on the origin. The coordinates of the points on the ring are $(q\sin\theta, q\cos\theta)$ for $\theta \in [0, 2\pi)$. The point P which is interacting with Q is located at $(0, g)$. The distance between P and Q is given by

$$\rho = \left[(q-g)^2 + 4gq\sin^2\frac{\theta_1}{2}\right]^{1/2},$$

and since the line element is $q\,d\theta$,

$$R_n = \int_0^{2\pi} q\left[(q-g)^2 + 4gq\sin^2\frac{\theta}{2}\right]^{-n} d\theta.$$

https://doi.org/10.1017/S1446181115000152 Published online by Cambridge University Press

By bisecting the interval of integration and making the substitution $t = \sin^2(\theta/2)$, we obtain

$$R_n = \frac{q}{2(q-g)^{2n}} \int_0^1 t^{-1/2}(1-t)^{-1/2}\left[1 + \frac{4gqt}{(q-g)^2}\right]^{-n} dt,$$

where the integral is of standard hypergeometric form. Note that the standard hypergeometric function is given by

$$F(a,b;c;z) = \frac{\Gamma(c)}{\Gamma(b)\Gamma(c-b)} \int_0^1 \frac{t^{b-1}(1-t)^{c-b-1}}{(1-tz)^a}\, dt.$$

Substituting the standard hypergeometric form into R_n yields

$$R_n = \frac{\pi q}{2(q-g)^{2n}} F\left(n, \frac{1}{2}; 1; -\frac{4gq}{(q-g)^2}\right),$$

and the total potential energy for P and Q is then given by

$$U_{PQ} = \frac{\pi\eta q}{2}\left[-\frac{C_1}{(q-g)^6} F\left(3, \frac{1}{2}; 1; -\frac{4gq}{(q-g)^2}\right) + \frac{C_2}{(q-g)^{12}} F\left(6, \frac{1}{2}; 1; -\frac{4gq}{(q-g)^2}\right)\right]. \tag{2.8}$$

To provide some variation on the location of point P for this case, we can consider the case where $P = (0, y_6, z_6)$ and is located on the yz-plane. To do this, we substitute $g = \sqrt{y_6^2 + z_6^2}$ into equation (2.8).

2.4.2. Point P located at the top or bottom of the ring The second case is when the point is interacting from the top or bottom of the ring. Using a three-dimensional coordinate system, the centre of the ring Q of radius q is located on the origin and the location of point P is (x_p, y_p, z_p). The coordinates of the points on the ring are $Q = (q\cos\theta, q\sin\theta, 0)$ for $\theta \in [0, 2\pi)$ and thus the distance between P and Q is given by

$$\rho = [\beta - \alpha q\cos(\theta - \theta_0),]^{1/2},$$

where $\beta = q^2 + x_p^2 + y_p^2 + z_p^2$, $\alpha = \sqrt{x_p^2 + y_p^2}$ and $\theta_0 = \arctan(y_p/x_p)$. To solve for R_n, we follow similar calculations to those of Tran-Duc et al. [15] and obtain

$$R_n = \int_0^{2\pi} q[\beta - \alpha q\cos(\theta - \theta_0)]^{-n}\, d\theta,$$
$$= \frac{2\pi q}{(\beta - \alpha q)^n} F\left(n, \frac{1}{2}; 1; \frac{2\alpha q}{\alpha q - \beta}\right),$$

and the potential energy for P_2 and Q is then given by

$$U_{PQ} = 2\pi\eta q\left[-\frac{C_1}{2(\beta - \alpha q)^3} F\left(3, \frac{1}{2}; 1; \frac{2\alpha q}{\alpha q - \beta}\right) + \frac{C_2}{120(\beta - \alpha q)^6} F\left(6, \frac{1}{2}; 1; \frac{2\alpha q}{\alpha q - \beta}\right)\right]. \tag{2.9}$$

In both cases, η is the mean atomic density of the ring which is calculated by dividing the number of atoms by the circumference of the ring.

https://doi.org/10.1017/S1446181115000152 Published online by Cambridge University Press

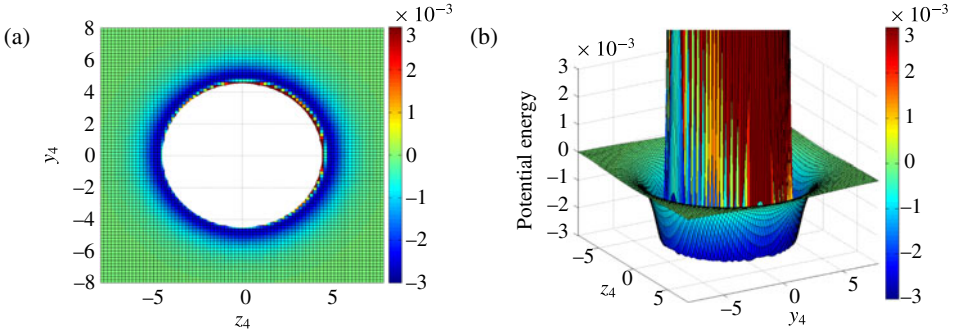

FIGURE 6. (Colour online) Contour plots of H interacting with a benzene ring from the side.

2.4.3. Benzene ring For the interaction of H with the benzene ring (C_6H_6), we assume that the centre of the benzene ring lies on the origin O and that it is made of two rings: one to represent the hydrogen atoms and the other to represent the carbon atoms. The radius of the hydrogen ring, r_h, is 2.48 Å, and of the carbon ring, r_c, is 1.4 Å. The mean surface density for the hydrogen ring, η_{4h}, is deduced from $6/(2\pi r_h) = 0.385$ Å, and for the carbon ring, η_{4c}, is deduced from $6/(2\pi r_c) = 0.682$ Å. Parameters C_1 and C_2 for the hydrogen–carbon and hydrogen–hydrogen interactions can be found in Table 1. The total potential energy for H interacting with a benzene ring is calculated by adding up both the potential energies for H interacting with the hydrogen ring and carbon ring following equation (2.5), where U_C is the potential energy for H with the carbon ring, and U_H is the potential energy for H with the hydrogen ring.

For the case of H interacting with the benzene ring from the side, we assume that the position of the hydrogen atom is at $(0, y_4, z_4)$, and make the substitution $g = \sqrt{z_4^2 + y_4^2}$ into equation (2.8). The two-dimensional contour plot for this interaction is presented in Figure 6(a) and the three-dimensional contour plot in Figure 6(b). The most stable position for the hydrogen atom is at the blue section of the contour plots or at about 4.9 Å from the centre of the benzene ring.

For the case of H interacting with the benzene ring from the top (or bottom), we assume that the position of H is at $(1, y_4, z_4)$. The two-dimensional contour plot for this interaction is presented in Figure 7(a) and the three-dimensional contour plot in Figure 7(b). The most stable position for the hydrogen atom is at the blue section (colour online) of the contour plots or at about 1 Å from the centre of the benzene ring. The hydrogen atom experiences a repulsive force in the centre of the benzene ring, as shown by the red area (colour online) of the figures.

2.5. Interaction with a sphere For the interaction of an atom P with a sphere S of radius t, we assume that the centre of the sphere is at the origin O. Thus, the location of any point on the surface of the sphere in Cartesian coordinates is defined as

$$S_i = (t \sin\theta \cos\phi, t \sin\theta \sin\phi, t \cos\theta),$$

https://doi.org/10.1017/S1446181115000152 Published online by Cambridge University Press

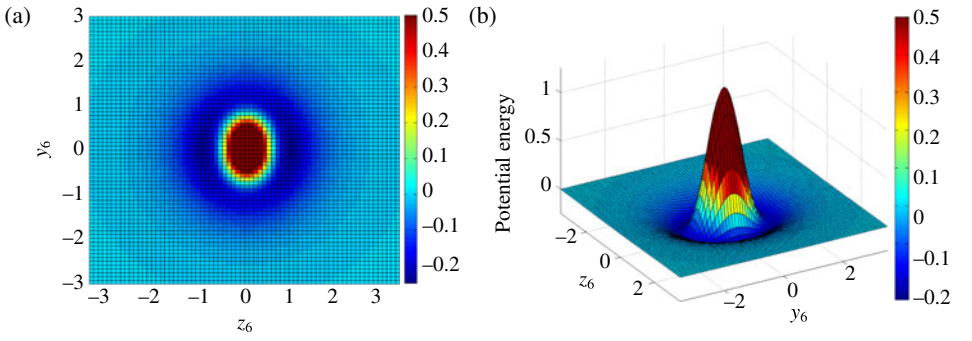

FIGURE 7. (Colour online) Contour plots of H interacting with a benzene ring from the top.

where ϕ is the azimuthal angle in the xy-plane with $\phi \in [-\pi, \pi)$ and θ is the zenith angle with $\theta \in [0, \pi]$.

To make the calculation easier, we assume that P lies on the z-axis and is at a distance g from the centre of S, and thus is defined as $(0, 0, g)$. The distance between P and S_i is

$$\rho = [t^2 \sin^2\theta + (t\cos\theta - g)^2]^{1/2},$$

and given that the area element is $t^2 \sin\theta \, d\phi \, d\theta$, R_n is calculated using methods similar to those of Cox et al. [4] as follows:

$$\begin{aligned} R_n &= \int_0^{\pi}\int_{-\pi}^{\pi} t^2 \sin\theta [t^2\sin^2\theta + (t\cos\theta - g)^2]^{-n} \, d\phi \, d\theta \\ &= \frac{\pi t}{g(1-n)}\left[\frac{1}{(t+g)^{2(n-1)}} - \frac{1}{(t-g)^{2(n-1)}}\right]. \end{aligned}$$

Substituting R_n into the potential energy equation (2.2) gives

$$U_{PS} = \frac{\pi\eta t}{g}\left[\frac{C_1}{2}\left\{\frac{1}{(g+t)^4} - \frac{1}{(g-t)^4}\right\} - \frac{C_2}{5}\left\{\frac{1}{(g+t)^{10}} - \frac{1}{(g-t)^{10}}\right\}\right], \tag{2.10}$$

where U_{PS} is the total potential energy of P interacting with S. The parameter η is the mean surface density for the sphere, which is calculated by dividing the number of atoms by the surface area of the sphere.

2.5.1. Interaction inside and outside a sphere There are two different cases for the interaction of P with a sphere: (i) P is located inside the sphere; and (ii) P is located outside the sphere. To account for the position of P inside and outside the sphere, we redefine the position of P to be located on the yz-plane such that the position of P is $(0, y_p, z_p)$.

Substituting $g = \sqrt{y_p^2 + z_p^2}$ into equation (2.10) will provide the interaction energy between P and S. If P is inside the sphere, then the distance of P from the centre of S has to be smaller than its radius such that $g < t$. If P is located outside the sphere, then $g > t$.

https://doi.org/10.1017/S1446181115000152 Published online by Cambridge University Press

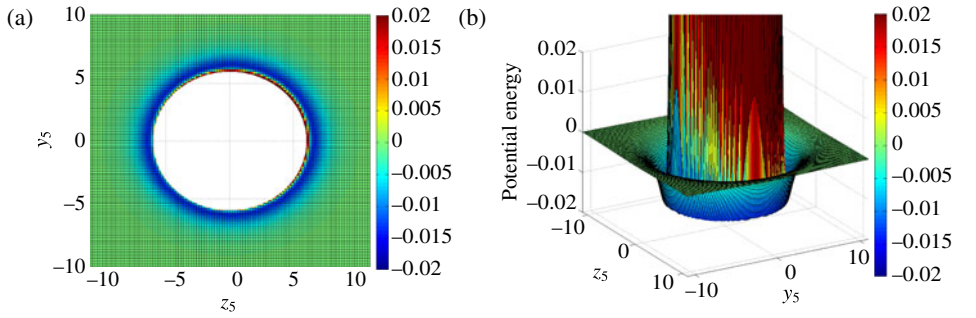

FIGURE 8. (Colour online) Contour plots of H interacting the outer walls of a C_{60} fullerene.

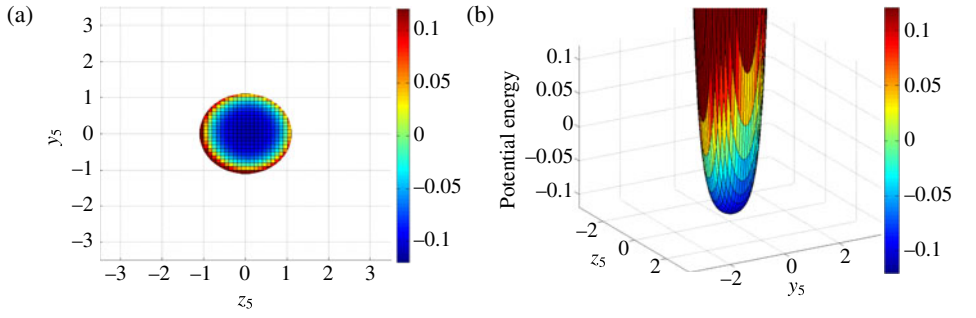

FIGURE 9. (Colour online) Contour plots of H interacting with the inner walls of a C_{60} fullerene.

2.5.2. Fullerene In this section, we demonstrate the interaction between a hydrogen atom and a fullerene (C_{60}). We present the two cases where the hydrogen atom is located inside and outside the fullerene. We assume that H is located at $(0, y_5, z_5)$ and the centre of the fullerene is at the origin O. Here we use equation (2.10) to generate a three-dimensional figure. The mean surface density for a fullerene, $\eta_5 = 60/(4\pi t^2) = 0.379\,\text{Å}^{-2}$, where $t = 3.55\,\text{Å}$ is the radius of the fullerene. The parameters C_1 and C_2 for the hydrogen–carbon interactions can be found in Table 1.

Figure 8 shows the contour plots of the potential energy of a hydrogen interacting outside a C_{60}. The minimum potential energy occurs in the dark blue sections of the contour plots or at 6.5 Å from the centre of the fullerene.

Figure 9 shows the contour plots of the potential energy of a hydrogen interacting inside a C_{60}. The minimum potential energy, in this case, occurs in the centre of the fullerene due to the small size of the fullerene. If H is interacting with a larger sphere, the minimum potential energy will be located nearer to the walls of the fullerene and away from the centre.

2.6. Interaction with an infinite cylinder The last building block that is described is the cylinder. Point P is located on the xy-plane at $(g, 0, 0)$ and the cylindrical surface C is defined to be $(c\cos\theta, c\sin\theta, z_c)$ where c is the radius of the cylinder, $\theta \in [0, 2\pi)$,

https://doi.org/10.1017/S1446181115000152 Published online by Cambridge University Press

$z_c \in (-\infty, \infty)$. We present two cases in the following subsections where: (i) point P is located inside the cylinder; and (ii) point P is located outside the cylinder.

2.6.1. Point P located inside cylinder For this case, $g < c$. The distance from P to C is thus given by

$$\begin{aligned}\rho_1 &= [(c\cos\theta - g)^2 + c^2\sin^2\theta + z_c^2]^{1/2} \\ &= [(c-g)^2 + z_c^2 + 4cg\sin^2(\theta/2)]^{1/2}.\end{aligned}$$

The area element is given by $c\,d\theta\,dz_c$ which is used to solve for R_{n1}. Following similar calculations of Cox et al. [4], we obtain

$$\begin{aligned}R_{n1} &= \int_{-\infty}^{\infty}\int_{-\pi}^{\pi} c[(c-g)^2 + z_c^2 + 4cg\sin^2(\theta/2)]^{-n}\,d\theta\,dz_c \\ &= c\int_{-\pi}^{\pi}\frac{1}{\alpha^{2n-1}}\,d\theta\int_{-\pi/2}^{\pi/2}\cos^{2n-2}\psi\,d\psi,\end{aligned}$$

where $\alpha^2 = (c-g)^2 + 4cg\sin^2(\theta/2)$. Further, substituting $t = \sin^2(\theta/2)$ yields

$$R_{n1} = \frac{2c}{(c-g)^{2n-1}}B\left(n-\frac{1}{2},\frac{1}{2}\right)\int_0^1 t^{-1/2}(1-t)^{-1/2}\left(1+\frac{4cgt}{(c-g)^2}\right)^{(1/2)-n}dt,$$

which by using Euler's integral formula reduces to

$$\begin{aligned}R_{n1} &= \frac{2\pi c}{(c-g)^{2n-1}}B\left(n-\frac{1}{2},\frac{1}{2}\right)F\left(n-\frac{1}{2},\frac{1}{2};1;-\frac{4cg}{(c-g)^2}\right) \\ &= \frac{2\pi^2}{\Gamma(2n-1)(2c)^{2n-2}}\sum_{m=0}^{\infty}\left(\frac{\Gamma(2n+2m-1)g^m}{\Gamma(n+m)m!(4c)^m}\right)^2.\end{aligned}$$

We can now express the total potential energy between C and P as

$$U_{CP_1} = \frac{\pi^2\eta_6}{192}(-C_1R_3 + C_2R_6), \tag{2.11}$$

where

$$\begin{aligned}R_3 &= \frac{1}{c^4}\sum_{m=0}^{\infty}\left[\frac{(2m+4)!g^m}{(m+2)!m!(4c)^m}\right]^2, \\ R_6 &= \frac{1}{9\,676\,800c^{10}}\sum_{m=0}^{\infty}\left[\frac{(2m+10)!g^m}{(m+5)!m!(4c)^m}\right].\end{aligned}$$

2.6.2. Point P located outside cylinder The second case is when point P is outside the cylinder, that is, $g > c$. In this case, the distance from P to C is

$$\begin{aligned}\rho_2 &= [(g - c\cos\theta)^2 + c^2\sin^2\theta + z_c^2]^{1/2} \\ &= [(g-c)^2 + z_c^2 + 4cg\sin^2(\theta/2)]^{1/2}.\end{aligned}$$

https://doi.org/10.1017/S1446181115000152 Published online by Cambridge University Press

We perform calculations similar to those above to solve for the integral

$$R_{n2} = \int_{-\infty}^{\infty}\int_{-\pi}^{\pi} c[(g-c)^2 + z_c^2 + 4cg\sin^2(\theta/2)]^{-n}\, d\theta\, dz_c$$

to yield

$$\begin{aligned} R_{n2} &= \frac{2c\pi}{(g-c)^{2n-1}} B\Big(n-\frac{1}{2},\frac{1}{2}\Big) F\Big(n-\frac{1}{2},\frac{1}{2};1;-\frac{4cg}{(g-c)^2}\Big) \\ &= \frac{4c\pi^2}{\Gamma(2n-1)(2g)^{2n-1}} \sum_{m=0}^{\infty}\Big[\frac{\Gamma(2n+2m-1)c^m}{\Gamma(n+m)m!(4g)^m}\Big]^2. \end{aligned}$$

Thus, the total potential energy between C and P is

$$U_{CP_2} = \frac{c\pi^2\eta_6}{192}(-C_1 R_3 + C_2 R_6), \tag{2.12}$$

where

$$\begin{aligned} R_3 &= \frac{1}{g^5}\sum_{m=0}^{\infty}\Big[\frac{(2m+4)!c^m}{(m+2)!m!(4g)^m}\Big]^2, \\ R_6 &= \frac{1}{9\,676\,800g^{11}}\sum_{m=0}^{\infty}\Big[\frac{(2m+10)!c^m}{(m+5)!m!(4g)^m}\Big]^2. \end{aligned}$$

In both cases, η_6 is the mean atomic density for the cylinder, which is calculated by dividing the number of atoms by the surface area of the cylinder.

To provide some variation on the location of point P, we can consider the case where $P = (0, y_6, z_6)$ and is located on the yz-plane. Here we substitute $g = \sqrt{y_6^2 + z_6^2}$ into equation (2.11) to obtain the potential energy inside the cylinder and into equation (2.12) to obtain the potential energy outside the cylinder.

2.6.3. Carbon nanotube In this section, we model the interaction between a hydrogen atom and a semi-infinite (10,10) carbon nanotube of radius $c = 6.784$ Å. The mean surface density for a carbon nanotube is the same as for a graphene. Therefore, $\eta_6 = 4\sqrt{3}/(9\gamma^2) = 0.381$ A^{-2}, where $\gamma = 1.421$ Å is the carbon–carbon length. The value of the parameters C_1 and C_2 for the hydrogen–carbon interactions can be found in Table 1. For the case where H is located inside the carbon nanotube, we assume that H is located at $(0, y_6, z_6)$, and the centre of the carbon nanotube lies on the x-axis.

Substituting these parameter values into equation (2.11) shows the total potential energy between the hydrogen atom and the semi-infinite (10, 10) carbon nanotube as a function of y_6 and z_6. Figure 10 shows plots of this function. H is at equilibrium distance at 3.75 Å from the centre of the carbon nanotube as shown in the dark blue sections of the contour plots. The potential energy will tend to zero as H moves towards the centre of the nanotube.

Figure 11 shows the contour plots of the potential energy of H interacting outside an infinite carbon nanotube. The potential energy for this interaction is obtained by

https://doi.org/10.1017/S1446181115000152 Published online by Cambridge University Press

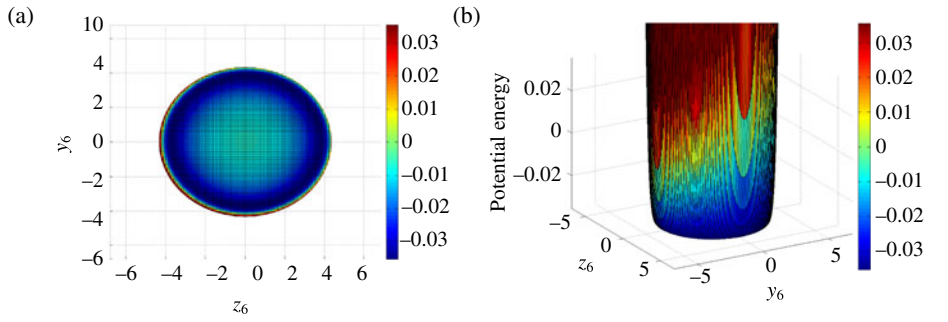

FIGURE 10. (Colour online) Contour plots of H interacting with the inner walls of an infinite carbon nanotube.

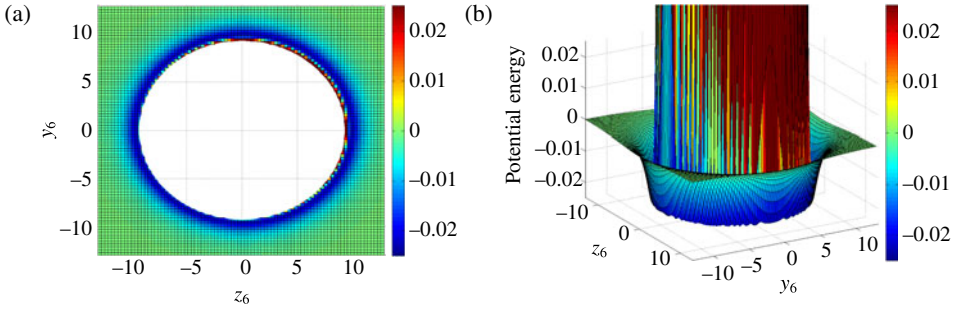

FIGURE 11. (Colour online) Contour plots of H interacting with the outer walls of an infinite carbon nanotube.

substituting the values of the parameters into equation (2.12). As shown in the figure, H is at equilibrium distance at 9.7 Å from the centre of the carbon nanotube as shown in the dark blue sections (colour online) of the contour plots.

3. Example of interactions with porous materials

In this section, we present some examples of how we can implement the idea of building blocks discussed in the previous sections. An example of how nanostructures can be represented by planes and rings has been given by Tran-Duc et al. [14]. This paper investigated the adsorption of polycyclic aromatic hydrocarbons – in particular, coronene ($C_{24}H_{12}$) – onto a graphite surface using both the discrete and continuous approach. The coronene is modelled as four circular rings and the graphite surface as a plane as shown in Figure 12. The equation for the potential energy between the two is based on equations (2.6) and (2.9).

Comparison of results obtained using the discrete and continuous method shows that the continuous method provides results that are as accurate as the discrete method. The energy profiles for the interaction between two structures are also provided for

https://doi.org/10.1017/S1446181115000152 Published online by Cambridge University Press

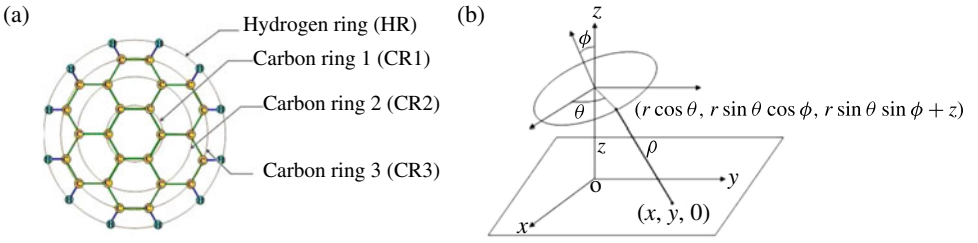

FIGURE 12. (Colour online) (a) Geometric representation of coronene ($C_{24}H_{12}$). (b) Coronene interacting with a graphite sheet. Reprinted from [14] with permission from Elsevier.

different values of the vertical distance between $C_{24}H_{12}$ and the graphene sheet Z. The different values used are: $Z \geq 7.5$ Å when it is far from the graphite surface; 3.9 Å $< Z < 7.5$ Å when it is at an intermediate distance; and $Z \leq 3.9$ Å when it is near the graphite plane. The authors concluded that the most stable configuration for coronene molecule when $Z \geq 7.5$ Å is when it is perpendicular to the graphene sheet. At 3.9 Å $< Z < 7.5$ Å a tilted configuration is preferred, and at $Z \leq 3.9$ Å the minimum potential energy occurs when it is parallel to the plane.

The spherical model is used in the paper by Thornton et al. [13] where the gas uptake for three types of MOFs is predicted: MOF-177, MOF-177 impregnated with C_{60} fullerenes (C_{60}@MOF) and MOF-177 impregnated with magnesium-decorated fullerenes (Mg–C_{60}@MOF). The paper first verified the model which is based on equation (2.10) with other experimental and simulation results. The authors reported that the model accurately portrays the observed effects of temperature, pressure and cavity size on hydrogen uptake. The model is then used to predict the hydrogen and methane uptake for MOF-177 and the proposed structures C_{60}@MOF and Mg–C_{60}@MOF by first calculating the potential energy within the cavity. In C_{60}@MOF and Mg–C_{60}@MOF the fullerene and magnesium-decorated fullerene are assumed to be located in the middle of the MOF structure and modelled as a sphere as shown in Figure 13(a). Figure 13(b) shows the potential energy gradient inside the Mg–C_{60}@MOF. The total potential energy is calculated by adding the potential energy between the gas and the MOF structure to the potential energy between the gas and the fullerene or magnesium-decorated fullerene. The authors in [13] concluded that Mg–C_{60}@MOF has a greater potential energy compared to the other structures and, therefore, is able to adsorb gases more efficiently.

The final example that is presented is the work by Adisa et al. [1] which discusses the encapsulation of methane molecules into carbon nanotubes using two different models of methane. The first model describes the methane molecule using the discrete method as shown in Figure 14(a). This model calculates the individual potential energy between the atoms on the methane and the carbon nanotube, which is modelled using the continuous approximation and is based on equations (2.11) and (2.12). The second model, as shown in Figure 14(b), assumes that the hydrogen atoms on the methane are evenly distributed over the surface of a sphere with the carbon atom at its centre

https://doi.org/10.1017/S1446181115000152 Published online by Cambridge University Press

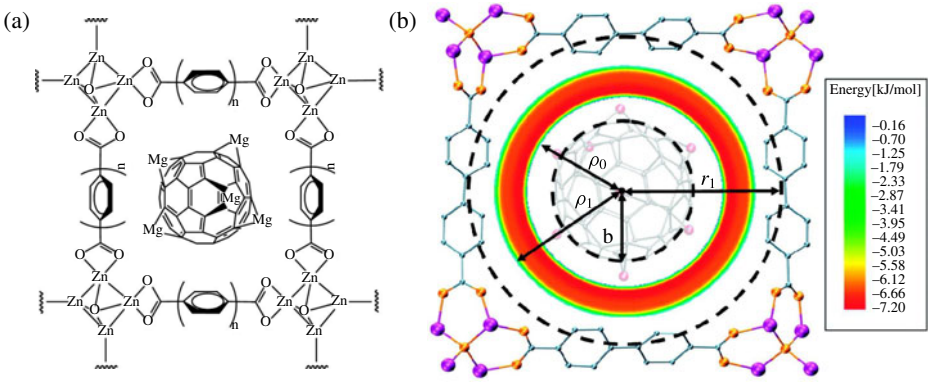

FIGURE 13. (Colour online) MOF-177 impregnated with magnesium-decorated fullerenes (Mg–C_{60}@MOF). The schematic representation for Mg–C_{60}@MOF is given in (a) and the potential energy for adsorption in the cavity is described in (b). Reprinted with permission from [13]; copyright 2009 American Chemical Society.

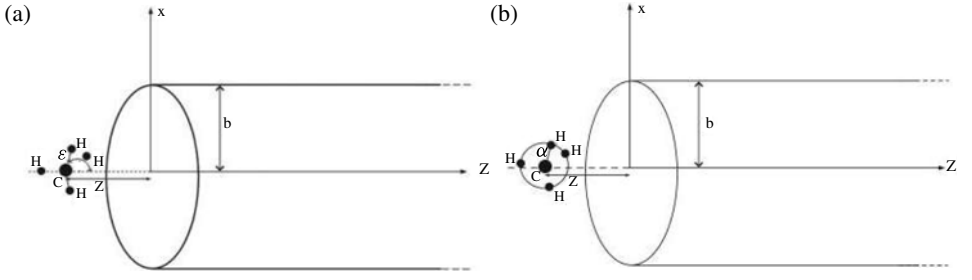

FIGURE 14. Two different representations of a methane molecule entering a carbon nanotube: (a) discrete representation of the methane molecule; (b) continuous representation of the methane molecule. Reprinted from [1] with permission from Elsevier.

and is based on equation (2.10). The potential energy between the methane molecule and carbon nanotube is then calculated by adding the potential energy of the carbon atom and the carbon nanotube using the discrete method and the potential energy of the hydrogen atoms and the carbon nanotube using the continuous approximation. Comparison between the two models shows that the continuous approximation, which is a simpler way to calculate the potential energy, produces comparable results to the discrete model.

4. Conclusions

We determine analytical potential energy models which describe the interactions between atoms and various idealized building blocks, such as points, lines, planes, rings, spheres and cylinders. Case studies of these models provide the potential energy distribution between a hydrogen atom and various building blocks represented by

https://doi.org/10.1017/S1446181115000152 Published online by Cambridge University Press

a carbon atom, polyacetylene, graphene sheet, benzene ring, fullerene and carbon nanotube. It is important to note that the analytical models can be combined to represent more complicated structures. Examples of structures that represent a combination of the analytical models to determine the total potential energy between the interacting structures [1, 13, 14] have been discussed. Describing complicated structures using idealized building blocks allows us to simplify the model, so that calculations can be done easily and accurately.

The analytical method presented here approximates the interactions between the atoms on the building blocks and the gas molecules, particularly for those structures that have uniformly distributed atoms. Even for nonuniformly distributed atoms, this technique provides an average approximation as shown by Thornton et al. [13]. In that paper, MOF-177 is modelled as a sphere by smearing the atoms of the structure, which are a mixture of zinc, carbon, oxygen and hydrogen, over the surface of a sphere, and the adsorption isotherms from the analytical model agree well with experimental isotherms.

We have only described some idealized building blocks that are regular in shape. However, fortunately for porous materials that are irregularly shaped, their pores can still be represented using cylindrical, spherical or slit-shaped porosity, since these are used for all pore size characterization methods which include permporometry, thermoporometry, mercury intrusion, positron annihilation, lifetime spectroscopy and gas adsorption and (or) desorption methods [8]. To date, there has been no geometric representation of nanoporous structures that are cubic or parallelepipeds, and further work is currently in progress to present analytical models using parallelepipeds to represent materials, such as MOF-5 which has a cubic structure.

Acknowledgements

This work is partially supported by the Australian Research Council Discovery Project Scheme. The first author is grateful for a scholarship from The University of Adelaide and CSIRO Division of Material Science and Engineering.

References

[1] O. O. Adisa, B. J. Cox and J. M. Hill, "Encapsulation of methane molecules into carbon nanotubes", *Physica B* **406** (2011) 88–93; doi:10.1016/j.physb.2010.10.027.

[2] U. Bossel, "Does a hydrogen economy make sense?", *Proc. IEEE* **94** (2006) 1826–1837; doi:10.1109/JPROC.2006.883715.

[3] H. M. Cheng, Q. H. Yang and C. Liu, "Hydrogen storage in carbon nanotubes", *Carbon* **39** (2001) 1447–1454; doi:10.1016/S0008-6223(00)00306-7.

[4] B. J. Cox, N. Thamwattana and J. M. Hill, "Mechanics of atoms and fullerenes in single-walled carbon nanotubes. I. Acceptance and suction energies", *Proc. R. Soc. Lond. A* **463** (2007) 461–477; doi:10.1098/rspa.2006.1771.

[5] J. E. Lennard-Jones, "Cohesion", *Proc. Phys. Soc.* **43** (1931) 461–482; doi:10.1088/0959-5309/43/5/301.

[6] J.-R. Li, R. J. Kuppler and H.-C. Zhou, "Selective gas adsorption and separation in metal-organic frameworks", *Chem. Soc. Rev.* **38** (2009) 1477–1504; doi:10.1039/b802426j.

[7] W.-X. Lim, A. W. Thornton, A. J. Hill, B. J. Cox, J. M. Hill and M. R. Hill, "High performance hydrogen storage from Be-BTB metal-organic framework at room temperature", *Langmuir* **29** (2013) 8524–8533; doi:10.1021/la401446s.

[8] S. Lowell, J. E. Shields, M. A. Thomas and M. Thommes, *Characterization of porous solids and powders: surface area, pore size and density*, Volume 16 of *Particle Technology Series* (Kluwer Academic, Dordrecht, 2004).

[9] L. J. Murray, M. Dincă and J. R. Long, "Hydrogen storage in metal-organic frameworks", *Chem. Soc. Rev.* **38** (2009) 1294–1314; doi:10.1039/b802256a.

[10] A. K. Rappe, C. J. Casewit, K. S. Colwell, W. A. Goddard III and W. M. Skiff, "UFF, a full periodic table force field for molecular mechanics and molecular dynamics simulations", *J. Amer. Chem. Soc.* **114** (1992) 10024–10035; doi:10.1021/ja00051a040.

[11] N. L. Rosi, J. Eckert, M. Eddaoudi, D. T. Vodak, J. Kim, M. O'Keeffe and O. M. Yaghi, "Hydrogen storage in microporous metal–organic frameworks", *Science* **300** (2003) 1127–1129; doi:10.1126/science.1083440.

[12] S. Satyapal, J. Petrovic, C. Read, G. Thomas and G. Ordaz, "The US Department of Energy's national hydrogen storage project: progress towards meeting hydrogen-powered vehicle requirements", *Catal. Today* **120** (2007) 246–256; doi:10.1016/j.cattod.2006.09.022.

[13] A. W. Thornton, K. M. Nairn, J. M. Hill, A. J. Hill and M. R. Hill, "Metal-organic frameworks impregnated with magnesium-decorated fullerenes for methane and hydrogen storage", *J. Amer. Chem. Soc.* **131** (2009) 10662–10669; doi:10.1021/ja9036302.

[14] T. Tran-Duc, N. Thamwattana, B. J. Cox and J. M. Hill, "Adsorption of polycyclic aromatic hydrocarbons on graphite surfaces", *Comput. Mater. Sci.* **49** (2010) S307–S312; doi:10.1016/j.commatsci.2010.03.001.

[15] T. Tran-Duc, N. Thamwattana, B. J. Cox and J. M. Hill, "Modelling the interaction in a benzene dimer", *Philos. Mag.* **90** (2010) 1771–1785; doi:10.1080/14786430903476349.

[16] T. Watanabe and D. S. Sholl, "Accelerating applications of metal–organic frameworks for gas adsorption and separation by computational screening of materials", *Langmuir* **28** (2012) 14114–14128; doi:10.1021/la301915s.